NANO LETTERS

Letter

pubs.acs.org/NanoLett

Hapticity-Dependent Charge Transport through Carbodithioate-Terminated [5,15-Bis(phenylethynyl)porphinato]zinc(II) Complexes in Metal−Molecule−Metal Junctions

Zhihai Li,[†] Manuel Smeu,[‡] Tae-Hong Park,[§] Jeff Rawson,[∥] Yangjun Xing,[†] Michael J. Therien,*[,∥] Mark A. Ratner,*[,‡] and Eric Borguet*[,†]

[†]Department of Chemistry, Temple University, Philadelphia, Pennsylvania 19122, United States

[‡]Department of Chemistry, Northwestern University, Evanston, Illinois 60208, United States

[§]Department of Chemistry, University of Pennsylvania, Philadelphia, Pennsylvania 19104, United States

[∥]Department of Chemistry, Duke University, Durham, North Carolina 27708, United States

Supporting Information

ABSTRACT: Single molecule break junction experiments and non-equilibrium Green's function calculations using density functional theory (NEGF-DFT) of carbodithioate- and thiol-terminated [5,15-bis(phenylethynyl)-10,20-diarylporphinato]zinc(II) complexes reveal the impact of the electrode-linker coordination mode on charge transport at the single-molecule level. Replacement of thiolate ($-S^-$) by the carbodithioate ($-CS_2^-$) anchoring motif leads to an order of magnitude increase of single molecule conductance. In contrast to thiolate-terminated structures, metal−molecule−metal junctions that exploit the carbodithioate linker manifest three distinct conductance values. We hypothesize that the magnitudes of these conductances depend upon carbodithioate linker hapticity with measured conductances across Au-[5,15-bis(4′-(dithiocarboxylate)phenylethynyl)-10,20-diarylporphinato]zinc(II)-Au junctions the greatest when both anchoring groups attach to the metal surface in a bidentate fashion. We support this hypothesis with NEGF-DFT calculations, which consider the electron transport properties for specific binding geometries. These results provide new insights into the origin of molecule-to-molecule conductance heterogeneity in molecular charge transport measurements and the factors that optimize electrode−molecule−electrode electronic coupling and maximize the conductance for charge transport.

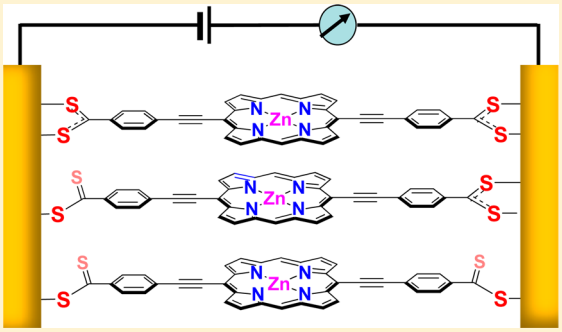

KEYWORDS: *Linker hapticity, STM break junction, NEGF-DFT, molecular electronics, carbodithioate linker*

Understanding electron transport through molecules is a prerequisite to the development of nanoscale and molecule-based devices.[1−7] Scanning tunneling microscopy (STM) break junction methods provide a powerful approach to determining single molecule conductances.[1,8−16] The choice of the linker moiety in metal−Molecule−metal (m−M−m) junctions, the so-called "alligator clip" that connects the molecular core to the electrode, plays a crucial role in determining transport characteristics,[9,11,17−20] as these units can shift the molecular core states relative to the metal Fermi energy as well as modulate the contact resistance.[11,20] While thiol is one of the most frequently used anchoring groups in m−M−m junctions because of its high affinity for Au surfaces,[21−23] recent studies demonstrate that an alternative sulfur-based linkage motif, carbodithioate, provides augmented electronic coupling and reduces the effective barrier for charge transport.[11,20] In this Letter, we utilize STM break junction measurements to contrast molecular conductances of [5,15-bis(4′-X-phenylethynyl)-10,20-diarylporphinato]zinc(II) [X = thiolate, S^-; carbodithioate, CS_2^-] complexes. This work not only further demonstrates the superior characteristics of carbodithioate relative to thiolate in molecular electronics applications: for the first time, it also reveals single molecule charge transport behavior across metal−Molecule−metal junctions attributed to the hapticity of the terminal CS_2^- moiety with the Au surface.

Terminally functionalized [5,15-bis(arylethynyl)-10,20-diaryl-porphinato]metal complexes[24−27] and their corresponding multi[(porphinato)metal] analogues that feature ethyne- and butadiyne-linked macrocyclic units provide minimal m−M−m resistances and offer exceptional utility in both molecular and nanoscale device architectures.[10,28−32] Figure 1A provides a schematic illustration of the STM break junction experiment, and Figure 1B shows the structures of two [5,15-bis((4′-X-phenyl)ethynyl)porphinato]zinc(II) complexes (X = S^-, −S-PZn-S−; X = CS_2^-, $-S_2C$-PZn-CS_2-). The design, synthesis, and characterization of these compounds, as well as details

Received: April 18, 2014
Revised: September 5, 2014
Published: September 25, 2014

   dx.doi.org/10.1021/nl502466a | *Nano Lett.* 2014, 14, 5493−5499

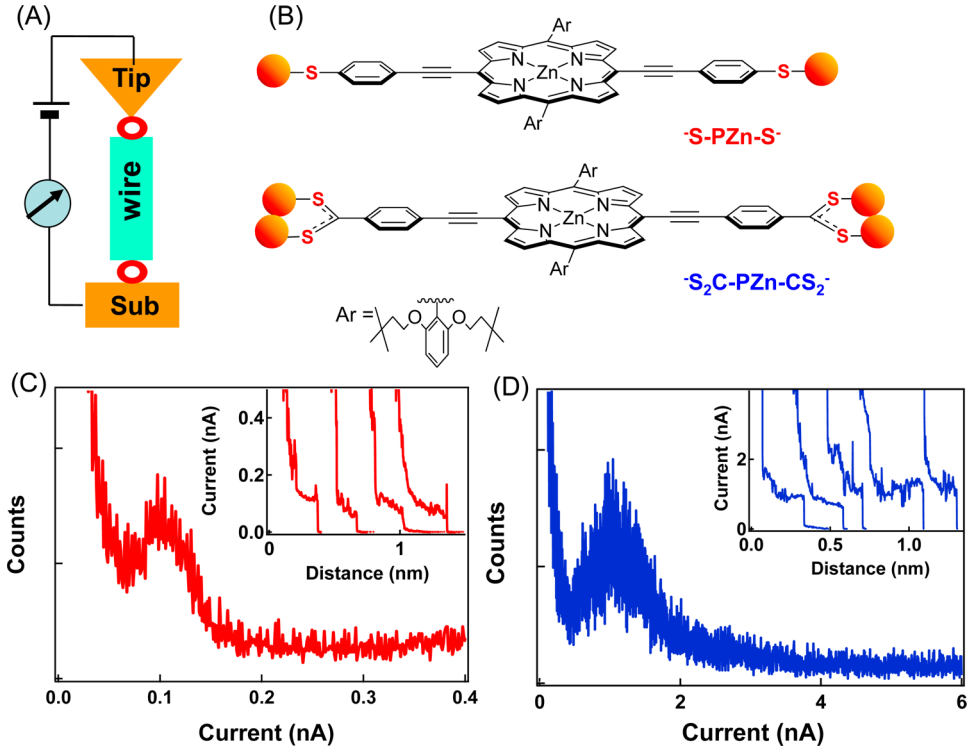

Figure 1. (A) Schematic illustration of STM break junction measurements. (B) Structures of [5,15-bis((4′-X-phenyl)ethynyl)-porphinato]zinc(II) complexes (X = S^-, −S-PZn-S−; X = CS_2^-, $-S_2C$-PZn-CS_2-). Respective current histogram analyses for (C) −S-PZn-S− (V_{bias} = 0.05 V, constructed with 208 stepped current−distance traces from 2000 total traces) and (D) $-S_2C$-PZn-CS_2- (V_{bias} = 0.05 V, constructed with 206 stepped current−distance traces from 2021 total traces). Inset: Examples of individual current−distance stepped traces recorded during STM break junction experiments.

concerning the STM break junction experiments, are described in the Supporting Information. In brief, the STM tip is driven into contact with the substrate and then retracted to break the metal contact. The current first decreases exponentially as the tip−substrate separation increases. In this process, current steps can be observed before the current drops down toward zero (Figure 1C,D insets). The current steps represent molecular junctions formed between the two electrodes (Figure 1A).[1,3,10,33] The histogram analysis of the data obtained for −S-PZn-S−, displayed in Figure 1C, shows a current maximum of 0.11 ± 0.02 nA at V_{bias} = 0.05 V, corresponding to a molecular conductance of 2.2 ± 0.3 nS.[10,31] An analogous histogram analysis (Figure 1D) for $-S_2C$-PZn-CS_2-, along with examples of current−distance traces recorded during the STM break junction experiments, show a current maximum near 1.15 nA. A linear fit of the resultant current values versus V_{bias} (Supporting Information Figure S5B, inset) obtained from these experiments reveals a single molecule conductance of 23 ± 2.1 nS for $-S_2C$-PZn-CS_2-. This value is 1 order of magnitude greater than that determined for −S-PZn-S−, and the conductance determined for a molecule with a similar (porphinato)zinc core terminated with two thiol groups.[10] Furthermore, these results are consistent with extensive experimental and theoretical data that examined the origin of the enhanced single molecule conductances observed for carbodithioate-terminated oligo-(phenyleneethynylene)s relative to corresponding structures that featured thiolate anchoring groups.[11]

For most current−distance traces recorded for $-S_2C$-PZn-CS_2--based m−M−m junctions, only a single type of current step was observed in the low current range (Figure 1D, Supporting Information Figure S5A). Unusual current plateaus, however, are observed for a small number of traces (Figure 2A; Supporting Information Figure S6B); these correspond to conductances much lower in magnitude than the typically observed value of 23 nS. Such low current steps appear at current plateaus of 0.6 and 0.12 nA, as indicated by the blue and black ovals (Figure 2A); these lower current steps are denoted as M (medium) and S (small). In order to reveal the properties of these current steps, we constructed another current histogram (Figure 2B) from traces exhibiting at least one of these M and S type steps (at V_{bias} = 0.05 V). While the current peak associated with the conductance of 23 nS is observed at 1.15 nA (red arrow in Figure 2B), the M and S steps present additional current peaks around 0.6 nA (blue arrow) and 0.12 nA (black arrow), corresponding to single molecule conductances of 12 and 2.4 nS, respectively (Figure 2). Note that the M and S steps are "infrequent", that is, observed approximately five times less often than normal current plateaus (Table 1). With respect to these M and S traces, it is found that (1) The probability of observing traces with M or S current steps is much lower than that of observing traces with normal steps (denoted as "N"). Approximately 2% of all individual current−distance stepped traces recorded during these STM break junction experiments display M and/or S type steps following N type steps; in contrast, ∼10% of the individual current−distance stepped traces show only N type steps (Table 1, Figure S6 in Supporting Information). (2) The M and S current steps almost always appear after the observation of "normal" (N) current steps. From a total of 2021 recorded current-distance traces, only three traces display the low current steps without accompanying N steps (Table 1,

dx.doi.org/10.1021/nl502466a | Nano Lett. 2014, 14, 5493−5499

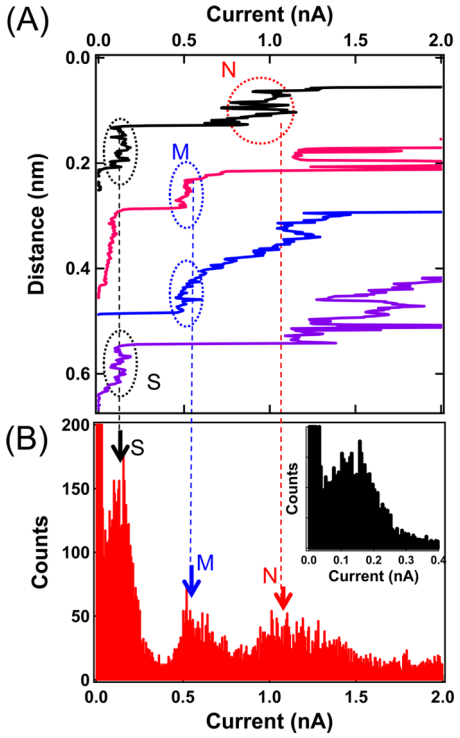

Figure 2. (A) Sample current−distance traces displaying "low" current steps during the STM break junction measurements of $-S_2C$-PZn-CS_2- (V_{bias} = 0.05 V). The red circle indicates a "normal" current step (N), while the blue and black ovals designate respectively two types of infrequent current steps, M (medium) and S (small). (B) Current histogram for current−distance traces displaying the M and S steps. Inset: expansion of low current region (black oval). The three peaks indicated by the arrows correspond to conductances of 23 (red), 12 (blue), and 2.4 nS (black), respectively.

Table 1. Statistical Distribution of the Current-Distance Stepped Traces Recorded for $-S_2C$-PZn-CS_2- (V_{bias} = 0.05 V)

total recorded current−distance traces	number (and fraction) of current−distance stepped traces that feature N, both N and M or S, and M and/or S only current steps[a]		
measured	N only	Both N and (M or S)	M and/or S only
2021	206 (10%)	41 (2%)	3 (0.15%)

[a]N, M, S denote normal, medium, and small current steps, respectively.

~0.15% of all recorded traces), an order of magnitude fewer than the number of traces that feature an N step with either M or S type steps (2%).

To probe the impact of the coordinating group upon molecular conductance, we compared statistical data and conductance values determined for Au−S_2C-PZn-CS_2−Au junctions with those measured for analogous junctions using thiol linkers.[3,8,12,34,35] Multiple conductance values have been observed previously for some m−M−m junctions that featured thiol anchoring groups,[3,8] including *meso*-to-*meso* ethyne-bridged (porphinato)zinc(II) structures connected to gold electrodes via (4′-thiophenyl)ethynyl termini.[31] Note that a distinguishing characteristic of previously established systems showing multiple single molecule conductances is that the probability of observing each of the values is similar. For example, when multiple conductance values were reported for alkanedithiol molecules, measurements of high or low conductances occurred with similar frequency and were attributed to the presence of similar populations of molecules that differed with respect to conformation.[8] Likewise, a high conductance/low conductance observation probability of 2:1 was ascribed to originate from differing molecule−electrode contact geometries.[3] In general, for m−M−m systems in which multiple single molecule conductance values are observed with similar probability, the most frequently observed conductance is assigned to Au−molecule−Au junctions in which the molecule adopts the most stable configuration, contact geometry, or molecular orientation.[3,8,12,34,35] In this study, the observation of low current steps for $-S_2C$-PZn-CS_2- occurs rarely (2% of all traces, Table 1) relative to the observation of normal (N) stepped traces (10% of all traces, Table 1). The infrequency with which current−distance traces that feature M or S steps are observed suggests that they have origins distinct from multiple single molecule conductance values observed with comparable probability in previously studied systems.

One might think that the N-M-S transitions stem from electrode interactions with the π-symmetric molecular orbitals of $-S_2C$-PZn-CS_2-,[36,37] which would be relevant at shorter electrode-electrode separations, but work by Kiguchi et al.[37] and Aradhya et al.[38] suggests that the electrode-molecule π interaction is substantially weaker (by 2 orders of magnitude) compared to the Au−S interaction.[36] Therefore, it is unlikely that the M and S conductance values correspond to π-interactions.

Finally, it is not reasonable to attribute the genesis of the three current peaks in Figure 2B to junctions in which two or multiple molecules are trapped; for such a scenario, the higher peak current values (M, N) should be integer multiples of the smallest current value (S),[1,3,8,19] that is, M should be equal to twice S, and N should be 3 times as high as S. Furthermore, to ascribe current/conductance peaks to junctions featuring multiple molecules, the lowest current value should occur with the highest probability.[1,3,8] The current−distance stepped trace data chronicled in Figure 2 and Table 1 for Au−S_2C-PZn-CS_2−Au junctions that feature M and S steps clearly do not derive from junctions that feature multiple molecules, as the "normal" (N) steps, which display the highest conductance, occur with the highest probability.

On the basis of these considerations, we ascribe the N, M, and S current steps to hapticity-dependent single molecule conductances that derive from the possible bidentate/bidentate, bidentate/monodentate, and monodentate/monodentate ligand interactions of the terminal CS_2^- moieties with the Au surface (Figure 3). In this model, the "normal" metal−molecule−metal junction formed during the STM break junction experiment corresponds to the case where the $-S_2C$-PZn-CS_2- molecule bridges two gold electrodes via bidentate interactions of both carbodithioate anchoring groups[39,40] (Figure 3A) and gives rise to the N-type current step at 23 nS. The M and S steps would then reflect partial breaking of electrode−carbodithioate bonds during the extension of molecular junctions (Figure 3B,C). Such partial breaking gives rise to Au−S_2C-PZn-CS_2−Au junctions in which one or both of the carbodithioate anchors interact with the Au surface in a monodentate fashion, a contact configuration analogous to the thiolate−Au contact; note in this regard that monodentate metal−carbodithioate ligation is well established.[41] Further satisfying aspects of this hypothesis include (i) the probability of interrogating the various m−M−m

dx.doi.org/10.1021/nl502466a | *Nano Lett.* 2014, 14, 5493−5499

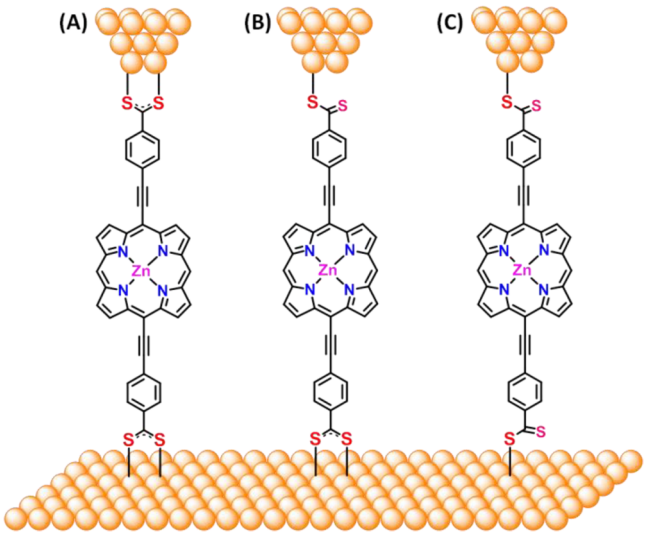

Figure 3. Schematic illustration of (A) bidentate/bidentate, (B) bidentate/monodentate, and (C) monodentate/monodentate carbodithioate–Au surface interaction modes for $-S_2C$-PZn-CS_2-. In this model, these three classes of Au–S_2C-PZn-CS_2–Au junctions respectively give rise to N, M, and S current steps.

junction configurations (Figure 3) tracks with chemical intuition in that a rigid, linear $-S_2C$-PZn-CS_2- molecule (Figure 1) should undergo partial breaking of the electrode–carbodithioate bond less frequently than complete breakage events, and (ii) it provides a simple rationalization of the relative magnitudes of the observed conductances: a bidentate/monodentate Au–S_2C-PZn-CS_2–Au junction (Figure 3B) results in a single molecule conductance (12 nS) of half that enabled by bidentate/bidentate junctions, while a monodentate/monodentate Au–S_2C-PZn-CS_2–Au junction (Figure 3C) gives rise to a single molecule conductance (2.4 nS) virtually identical to that provided by a Au–S–PZn-S–Au junction (2.2 nS).

In light of these results for the Au–S_2C-PZn-CS_2–Au junction, we re-examined single molecule conductance data obtained for a large family of oligo(phenylene-ethynylene) (OPE) molecules terminated with thiol and carbodithioate linkers.[11] Indeed, infrequent current–distance traces evince low current steps for carbodithioate-terminated OPEs (Supporting Information Figure S8), which we ascribe to OPE molecular junctions with partially broken carbodithioate bonds. Furthermore, computational studies of carbodithioate-terminated OPE molecules show that the monodendate carbodithioate sulfur-to-Au electrode interactions lead to a lower value of the molecular conductance relative to a corresponding junction characterized by a bidendate carbodithioate–Au surface interaction.[11]

Further support for carbodithioate hapticity-dependent conductances in these single molecule break junction experiments is provided by current–distance traces that show an exponential decrease of tunneling current that is interrupted by a low current M step, that is followed by an even higher current plateau value. In Figure 4A, the 0.55 nA current indicated by a blue arrow derives from a bidentate/monodentate Au–S_2C-PZn-CS_2–Au junction at a bias of 0.05 V; the following current step with a higher conductance value (indicated by a red arrow) stems from a hapticity change of monodentate to bidentate, resulting in a bidentate/bidentate Au–S_2C-PZn-CS_2–Au junction and a measured single molecule conductance of 24 nS. Congruent with this model, note that Au–S–PZn-S–Au junctions, which possess a [5,15-bis(phenylethynyl)-10,20-diarylporphinato]zinc(II) core identical to Au–S_2C-PZn-CS_2–Au junctions, do not display current–distance traces having discernible M and S steps.[31]

We further explore this hypothesis with quantum transport calculations employing the nonequilibrium Green's function technique with density functional theory (NEGF-DFT).[42,43] Using this approach, we carried out a simulation of an STM break junction experiment. The structure shown in Figure 5A was used to model the Au–S_2C-PZn-CS_2–Au junction, and we calculated the conductance properties as the separation between the Au electrodes was increased. The structure in Figure 5A was specifically chosen as an initial condition that may result in the three conductance values observed experimentally and particularly to attempt to reproduce the current–distance trace from Figure 4A.

The NEGF-DFT method provides us with the transmission function, which is the probability that an electron with a given energy will pass from one electrode, through the molecule, and into the other electrode. This can be related to the current when a bias is applied between the two electrodes, and the value of transmission at the Fermi energy, E_F, of the electrodes (at zero bias) is a good approximation to the low-bias conductance. The details of the structure relaxations and NEGF-DFT electron transport calculations are provided in the

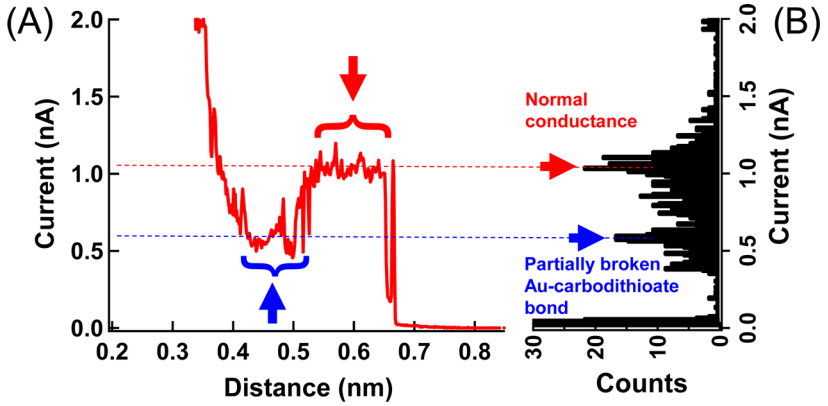

Figure 4. (A) A representative current–distance trace that highlights a current switch from M to N. (B) Conductance histograms from the three current–distance traces with two current steps/plateaus in which the high current step (N) followed a lower current (M) step.

dx.doi.org/10.1021/nl502466a | Nano Lett. 2014, 14, 5493–5499

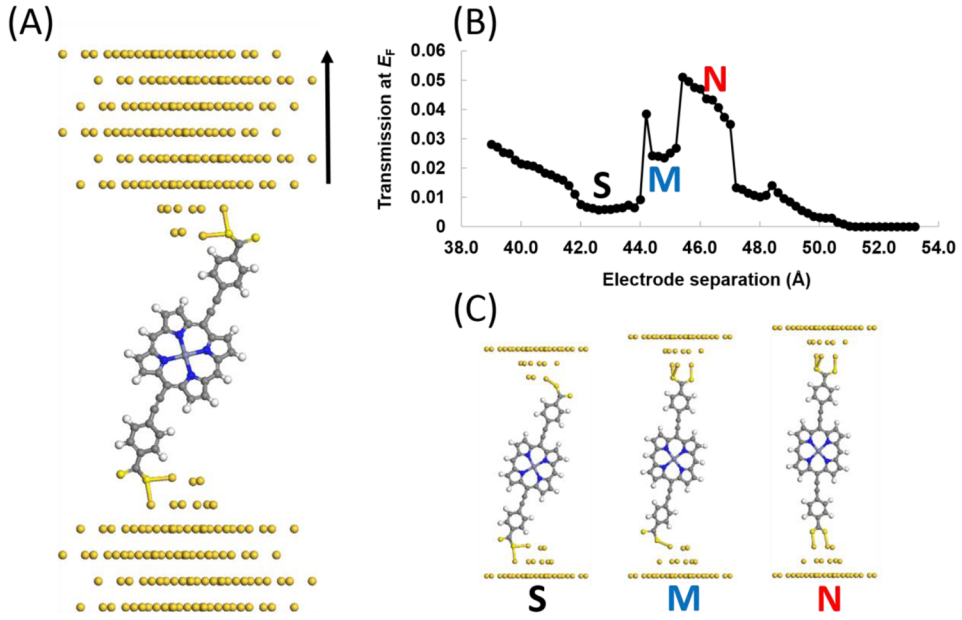

Figure 5. (A) Two-probe schematic structure used for the STM break junction simulations (NEGF-DFT). (B) Transmission at E_F as a function of electrode separation. S, M, and N represent small, medium, and normal conductance values, respectively, corresponding to the structures shown in (C). (C) Note that the electrode−electrode separation distance plays an important role in determining whether monodentate/monodentate (S), monodentate/bidentate (M), or bidentate/bidentate (N) configurations are favored.

Supporting Information. The transmission at E_F versus electrode separation is plotted in Figure 5B, with snapshots of the junction geometry at representative points shown in Figure 5C. Several plateaus where the transmission remains the same while the electrode separation increases by numerous 0.2 Å steps are marked as S, N, and M in Figure 5B. At the first and lowest of the three calculated plateaus, the molecule lies in a diagonal orientation, allowing only for monodentate/monodentate binding (S). The second plateau at intermediate transmission corresponds to a single bidentate linkage to the electrode (M). The third and highest plateau corresponds to bidentate links of the carbodithioate groups with their respective electrodes (N).

Notably, the ratios relating the measured N/M/S conductances and the three calculated plateau transmissions are similar. The highest transmission corresponds to the bidentate/bidentate configuration (N); there is a plateau having a transmission of about half this value, corresponding to the monodentate/bidentate configuration (M); and there is also a transmission plateau near one tenth the value of the highest transmission, and it corresponds to the monodentate/monodentate configuration (S). While we cannot know the exact $-S_2C$-PZn-CS_2- molecular configurations that are probed in these STM break junction experiments, the correspondence of the calculated transmissions with linker hapticities is compelling.

Figure 6 shows the transmission spectra (linear (B) and logarithmic (C) scales) for select carbodithioate−Au binding arrangements (A). We can see that as more and more S−Au bonds are formed, the transmission peaks near E_F become wider and the transmission values at E_F increase. The logarithmic plot (Figure 6C) reveals that the bidentate/bidentate configuration (red) manifests a higher transmission value at E_F than does the monodentate/bidentate (blue) configuration, which in turn displays a higher transmission value than the monodentate/monodentate (black) configuration. The m−M−m junction configuration just before the breaking point and the corresponding transmission peak are shown in green. An animation of the STM break junction simulation and a more in-depth analysis are available in the Supporting Information.

It should be stressed that from the experimental data, the N to M or S evolution was most commonly observed and occurs due to changes in bonding from bidentate to monodentate at one or both anchoring groups on the molecule. The bidentate/bidentate structure is likely the most commonly observed geometry due to the higher thermodynamic stability associated with this linkage motif. Structural changes that occur with increasing electrode−electrode separation during the experiment likely drive changes in anchoring group hapticity. Therefore, the exact distribution of molecular conductance states depends upon both the relative thermodynamic stabilities of the bidentate and monodentate linkages at a given electrode surface, as well as the geometric constraints as the electrodes are separated.

While the progression of N to M or S conductance can be explained in this manner, the trace shown in Figure 4A is counterintuitive because it shows an increase in conductance as the junction is stretched. For this reason, simulations were carried out to rationalize this rare experimental observation by selecting an initial special condition (Figure 5A) to allow the molecule to start in a low conductance orientation and progress through all three hapticity conditions and conductance values. The diagonal orientation of the molecule in the initial condition is a reasonable starting point that allows the molecule to begin in a monodentate/monodentate orientation and progress toward the bidentate/bidentate geometry as the electrode−electrode separation is increased and sufficient space is created for the molecule to adopt a vertical alignment, allowing additional bonds to form with the electrodes. It is important to note that the simulations only represent one conductance trace under very specific initial conditions aimed at reproducing a

dx.doi.org/10.1021/nl502466a | *Nano Lett.* 2014, 14, 5493−5499

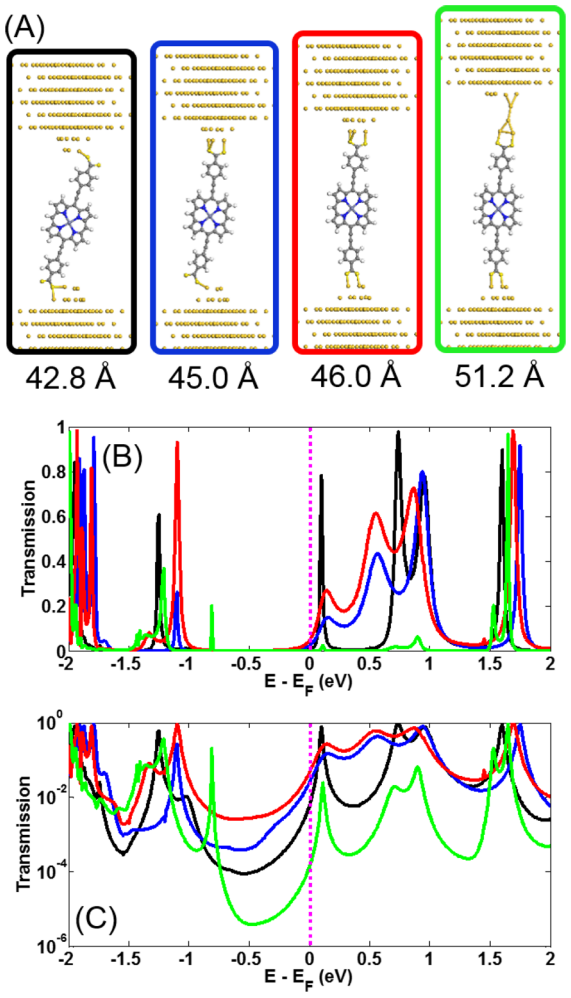

Figure 6. Transmission comparisons for selected electrode-electrode separation distances. (A) Four m−M−m junction binding configurations for $-S_2C$-PZn-CS_2-: monodentate/monodentate at 42.8 Å (black), monodentate/bidentate at 45.0 Å (blue), bidentate/bidentate at 46.0 Å (red), and the final structure before the junction breaks at 51.2 Å (green). (B) Transmission spectra (linear scale) for these m−M−m junction binding configurations. The plot line colors correspond to the border colors of structures shown in (A). (C) Transmission spectra displayed on a logarithmic scale. The value at the Fermi energy $E - E_F = 0$ is taken as the low-bias conductance (dashed purple line).

rare experimental observation (Figure 4A), and the simulated S-M-N progression has no statistical significance. The simulation, however, does confirm the existence of three conductance states that correlate with the possible bidentate/bidentate, bidentate/monodentate, and monodentate/monodentate ligand interactions of the terminal CS_2^- moieties with the Au surface at either electrode, in excellent agreement with the experimental data.

In summary, STM break junction experiments contrast the molecular conductances of two [5,15-bis((4′-X-phenyl)-ethynyl)-porphinato]zinc(II) (X = S^-, −S-PZn-S−; CS_2^-, $-S_2C$-PZn-CS_2-) complexes. These data highlight a single molecule conductance of 23 ± 2.1 nS for carbodithioate-anchored junctions, a value 10-fold greater than that determined for −S-PZn-S− molecules that exploit thiolate Au-surface linkers.[11,31] Current histogram analyses and detailed examination of thousands of current−distance traces reveal that Au−S_2C-PZn-CS_2−Au junctions display additional, infrequent single molecule conductances of 12 and 2.4 nS. We hypothesize that these lower conductance values derive respectively from Au−S_2-PZn-S_2−Au junctions in which one or both of the carbodithioate anchors interacts with the Au surface in a monodentate fashion (Figure 3). This hypothesis was investigated with NEGF-DFT electron transport calculations which showed good agreement with the hapticity-dependent conductance of the carbodithioate anchoring group. This work thus reveals hapticity-dependent single molecule conductances; furthermore, because the magnitude of the tunneling barrier depends upon carbodithioate linker hapticity, these experiments provide new insights into the origin of molecule-to-molecule conductance heterogeneity in molecular charge transport measurements, and the factors that optimize electrode−molecule−electrode electronic coupling and maximize the conductance and molecular switching.[44]

■ ASSOCIATED CONTENT

Supporting Information

Experimental details, conductance versus bias voltage measurements, current−distance traces for $-S_2C$-PZn-CS_2-, compound syntheses, and characterization data. Details of structure relaxations, NEGF-DFT electron transport calculations, and more in-depth analysis of the transmission properties of m−M−m junctions as a function of electrode−electrode separation. Movie of STM break junction simulation. This material is available free of charge via the Internet at http://pubs.acs.org.

■ AUTHOR INFORMATION

Corresponding Authors

*E-mail: michael.therien@duke.edu.
*E-mail: ratner@northwestern.edu.
*E-mail: eborguet@temple.edu.

Present Addresses

(Z.L.) Department of Chemistry, Ball State University, Muncie, IN 47306.
(T.H.P.) Nuclear Chemistry Research Division, Korea Atomic Energy Research Institute (KAERI), Daejeon, 305-353, Korea.

Notes

The authors declare no competing financial interest.

■ ACKNOWLEDGMENTS

E.B. thanks the National Science Foundation (CHE 0809838) for financial support. M.J.T. acknowledges the National Science Foundation (NSEC DMR04-25780) for infrastructural support and support of T.H.P.; M.J.T. is grateful to the UNC EFRC: Center for Solar Fuels, an Energy Frontier Research Center funded by the U.S. Department of Energy, Office of Science, Office of Basic Energy Sciences under Award Number DE-SC0001011, for its support of J.R. M.S. thanks the FRQNT for financial support and the Quest high-performance computing facility at Northwestern University. M.R. thanks the NSF (CHE 1058896) for financial support.

■ REFERENCES

(1) Xu, B. Q.; Tao, N. J. *Science* **2003**, *301*, 1221−1223.
(2) Vonlanthen, D.; Mishchenko, A.; Elbing, M.; Neuburger, M.; Wandlowski, T.; Mayor, M. *Angew. Chem., Int. Ed.* **2009**, *48*, 8886−8890.
(3) Li, X. L.; He, J.; Hihath, J.; Xu, B. Q.; Lindsay, S. M.; Tao, N. J. *J. Am. Chem. Soc.* **2006**, *128*, 2135−2141.
(4) Nitzan, A.; Ratner, M. A. *Science* **2003**, *300*, 1384−1389.

(5) Della Pia, E. A.; Chi, Q. J.; Jones, D. D.; Macdonald, J. E.; Ulstrup, J.; Elliott, M. *Nano Lett.* **2011**, *11*, 176−182.
(6) Lafferentz, L.; Ample, F.; Yu, H.; Hecht, S.; Joachim, C.; Grill, L. *Science* **2009**, *323*, 1193−1197.
(7) Roy, X.; Schenck, C. L.; Ahn, S.; Lalancette, R. A.; Venkataraman, L.; Nuckolls, C.; Steigerwald, M. L. *Angew. Chem., Int. Ed.* **2012**, *51*, 12473−12476.
(8) Li, C.; Pobelov, I.; Wandlowski, T.; Bagrets, A.; Arnold, A.; Evers, F. *J. Am. Chem. Soc.* **2008**, *130*, 318−326.
(9) Venkataraman, L.; Klare, J. E.; Nuckolls, C.; Hybertsen, M. S.; Steigerwald, M. L. *Nature* **2006**, *442*, 904−907.
(10) Sedghi, G.; Sawada, K.; Esdaile, L. J.; Hoffmann, M.; Anderson, H. L.; Bethell, D.; Haiss, W.; Higgins, S. J.; Nichols, R. J. *J. Am. Chem. Soc.* **2008**, *130*, 8582−8583.
(11) Xing, Y. J.; Park, T.-H.; Venkatramani, R.; Keinan, S.; Beratan, D. N.; Therien, M. J.; Borguet, E. *J. Am. Chem. Soc.* **2010**, *132*, 7946−7956.
(12) Zhou, X. S.; Liu, L.; Fortgang, P.; Lefevre, A. S.; Serra-Muns, A.; Raouafi, N.; Amatore, C.; Mao, B. W.; Maisonhaute, E.; Schollhorn, B. *J. Am. Chem. Soc.* **2011**, *133*, 7509−7516.
(13) Li, Z.; Borguet, E. *J. Am. Chem. Soc.* **2012**, *134*, 63−66.
(14) Huang, S.; He, J.; Chang, S. A.; Zhang, P. M.; Liang, F.; Li, S. Q.; Tuchband, M.; Fuhrmann, A.; Ros, R.; Lindsay, S. *Nat. Nanotechnol.* **2010**, *5*, 868−873.
(15) Arroyo, C. R.; Leary, E.; Castellanos-Gomez, A.; Rubio-Bollinger, G.; Gonzalez, M. T.; Agrait, N. *J. Am. Chem. Soc.* **2011**, *133*, 14313−14319.
(16) Kiguchi, M.; Takahashi, T.; Takahashi, Y.; Yamauchi, Y.; Murase, T.; Fujita, M.; Tada, T.; Watanabe, S. *Angew. Chem., Int. Ed.* **2011**, *50*, 5707−5710.
(17) Tam, E. S.; Parks, J. J.; Shum, W. W.; Zhong, Y. W.; Santiago-Berrios, M. B.; Zheng, X.; Yang, W. T.; Chan, G. K. L.; Abruna, H. D.; Ralph, D. C. *ACS Nano* **2011**, *5*, 5115−5123.
(18) Lortscher, E.; Cho, C. J.; Mayor, M.; Tschudy, M.; Rettner, C.; Riel, H. *ChemPhysChem* **2011**, *12*, 1677−1682.
(19) Chen, F.; Li, X. L.; Hihath, J.; Huang, Z. F.; Tao, N. J. *J. Am. Chem. Soc.* **2006**, *128*, 15874−15881.
(20) Tivanski, A. V.; He, Y. F.; Borguet, E.; Liu, H. Y.; Walker, G. C.; Waldeck, D. H. *J. Phys. Chem. B* **2005**, *109*, 5398−5402.
(21) Darwish, N.; Diez-Perez, I.; Da Silva, P.; Tao, N. J.; Gooding, J. J.; Paddon-Row, M. N. *Angew. Chem., Int. Ed.* **2012**, *51*, 3203−3206.
(22) Gonzalez, M. T.; Wu, S. M.; Huber, R.; van der Molen, S. J.; Schonenberger, C.; Calame, M. *Nano Lett.* **2006**, *6*, 2238−2242.
(23) Perrin, M. L.; Prins, F.; Martin, C. A.; Shaikh, A. J.; Eelkema, R.; van Esch, J. H.; Briza, T.; Kaplanek, R.; Kral, V.; van Ruitenbeek, J. M.; van der Zant, H. S. J.; Dulic, D. *Angew. Chem., Int. Ed.* **2011**, *50*, 11223−11226.
(24) LeCours, S. M.; DiMagno, S. G.; Therien, M. J. *J. Am. Chem. Soc.* **1996**, *118*, 11854−11864.
(25) LeCours, S. M.; Guan, H. W.; DiMagno, S. G.; Wang, C. H.; Therien, M. J. *J. Am. Chem. Soc.* **1996**, *118*, 1497−1503.
(26) Priyadarshy, S.; Therien, M. J.; Beratan, D. N. *J. Am. Chem. Soc.* **1996**, *118*, 1504−1510.
(27) LeCours, S. M.; Philips, C. M.; de Paula, J. C.; Therien, M. J. *J. Am. Chem. Soc.* **1997**, *119*, 12578−12589.
(28) Sedghi, G.; Garcia-Suarez, V. M.; Esdaile, L. J.; Anderson, H. L.; Lambert, C. J.; Martin, S.; Bethell, D.; Higgins, S. J.; Elliott, M.; Bennett, N.; Macdonald, J. E.; Nichols, R. J. *Nat. Nanotechnol.* **2011**, *6*, 517−523.
(29) Banerjee, P.; Conklin, D.; Nanayakkara, S.; Park, T. H.; Therien, M. J.; Bonnell, D. A. *ACS Nano* **2010**, *4*, 1019−1025.
(30) Conklin, D.; Park, T.-H.; Nanayakkara, D.; Therien, M. J.; Bonnell, D. A. *Adv. Funct. Mater.* **2011**, *21*, 4712−4718.
(31) Li, Z.; Park, T.-H.; Rawson, J.; Therien, M. J.; Borguet, E. *Nano Lett.* **2012**, *12*, 2722−2727.
(32) Conklin, D.; Nanayakkara, S.; Park, T.-H.; Lagadec, M. F.; Stecher, J.-T.; Therien, M. J.; Bonnell, D. A. *Nano Lett.* **2012**, *12*, 2414−2419.
(33) Hong, W.; Manrique, D. Z.; Garcia, P. M.; Gulcur, M.; Mishchenko, A.; Lambert, C. J.; Bryce, M. R.; Wandlowski, T. *J. Am. Chem. Soc.* **2012**, *134*, 2292−2304.
(34) Kamenetska, M.; Quek, S. Y.; Whalley, A. C.; Steigerwald, M. L.; Choi, H. J.; Louie, S. G.; Nuckolls, C.; Hybertsen, M. S.; Neaton, J. B.; Venkataraman, L. *J. Am. Chem. Soc.* **2010**, *132*, 6817−6821.
(35) Martin, S.; Haiss, W.; Higgins, S. J.; Nichols, R. J. *Nano Lett.* **2010**, *10*, 2019−2023.
(36) Wu, S. M.; Gonzalez, M. T.; Huber, R.; Grunder, S.; Mayor, M.; Schonenberger, C.; Calame, M. *Nat. Nanotechnol.* **2008**, *3*, 569−574.
(37) Kiguchi, M.; Tal, O.; Wohlthat, S.; Pauly, F.; Krieger, M.; Djukic, D.; Cuevas, J. C.; van Ruitenbeek, J. M. *Phys. Rev. Lett.* **2008**, *101*, 046801(1−4).
(38) Aradhya, S. V.; Frei, M.; Hybertsen, M. S.; Venkataraman, L. *Nat. Mater.* **2012**, *11*, 872−876.
(39) Colorado, R., Jr.; Villazana, R. J.; Lee, T. R. *Langmuir* **1998**, *14*, 6337−6340.
(40) Park, T.-H.; Therien, M. J. *Org. Lett.* **2007**, *9*, 2779−2782.
(41) Kano, N.; Kawashima, T. In *Topics in Current Chemistry*; Springer-Verlag: Berlin, 2005; Vol. *251*, p 141−180.
(42) Taylor, J.; Guo, H.; Wang, J. *Phys. Rev. B* **2001**, *63*, 245407(1−13).
(43) Waldron, D.; Haney, P.; Larade, B.; MacDonald, A.; Guo, H. *Phys. Rev. Lett.* **2006**, *96*, 166804(1−4).
(44) Li, Z.; Li, H.; Chen, S.; Froehlich, T.; Schenberger, C.; Calame, M.; Decurtins, S.; Liu, S.-X.; Borguet, E. *J. Am. Chem. Soc.* **2014**, *136*, 8867−8870.